AIAA JOURNAL
Vol. 30, No. 11, November 1992

Scale Effects in Buckling, Postbuckling, and Crippling of Graphite-Epoxy Z-section Stiffeners

Todd M. Wieland* and John Morton†
Virginia Polytechnic Institute and State University, Blacksburg, Virginia 24061
and
James H. Starnes Jr.‡
NASA Langley Research Center, Hampton, Virginia 23665

The buckling, postbuckling, and crippling of graphite-epoxy Z-section stiffeners are investigated as functions of specimen structural parameters. Variables addressed are flange and web widths, flange-to-web corner radii, thickness, and stacking sequence. Analytical, numerical, and experimental results are discussed. Nondimensional parameters have been obtained from an analytical model which effectively normalize the initial local buckling data reported herein and in the literature. The nature of the load redistribution after buckling is related to the geometric variables. A normalized total width concept is used to unify the crippling data. Crippling mechanisms include flange-free edge delamination and local failure of the flange-to-web corner and are shown to depend upon the laminate stacking sequence.

Introduction

THE implementation of composite materials in structural applications has involved the production of costly prototypes and large-scale experimental verification of certain design concepts. Scale-model testing can streamline the development process and help improve the cost-effectiveness of composite structures. Scale-model testing requires that the relationships between the responses of the small-scale model and full-size component be known so that the behavior of the model can be used to predict the responses of the full-size component. The relationships between the responses can be obtained through applied mechanics formulations. However, the presence of physical constraints or conflicts can prevent the complete reproduction of certain responses in small-scale models. Responses subject to such physical constraints or scaling conflicts include rate-dependent and notch-sensitive behaviors.[1] Furthermore, the mechanics formulations are still evolving for advanced material systems and may not provide the "scaling" relationships at the local material level necessary to relate all aspects of the response throughout the size range.

In the present study, a representative structural element has been selected which exhibits several response regimes of increasing complexity. The configuration is a laminated composite Z-section stiffener subjected to uniaxial, compressive loading. The response regimes are prebuckling, initial local buckling, postbuckling, and crippling. The configuration and response modes are relevant to a common aerospace design concept, in which a thin outer skin is reinforced by thin-walled stiffeners. Under compressive loads the skin and stiffeners may undergo local buckling. The structure may be required to carry additional load in the buckled configuration, necessitating the understanding of the structural behavior in the postbuckled response mode. The prebuckling and initial local buckling responses of the stiffener are readily modeled using available mechanics techniques. The postbuckling response involves increasing structural (geometric) and possibly material (constitutive) nonlinearities which add to the complexity of the mechanics problem and the solution techniques. The crippling response of stiffeners has been characterized phenomenologically, but the mechanics formulations of the process are still largely incomplete. Much analytical and experimental work addressing stiffener buckling and crippling has already been published (e.g., Refs. 2–7). Although the present work adds to this database of information, the primary purpose herein is to address the stiffener responses in the context of scaling. The objective of this work is to identify 1) the scaling relationships which govern the responses where possible, and 2) the responses which are either subject to scaling conflicts or inadequately modeled by the available mechanics formulations.

At least two approaches to a study in scaling are available. The first involves the use of dimensional analysis and similitude principles to define those nondimensional groups of geometric and material variables which govern the responses of scale models. From these parameters, an experimental program can be defined using a number of scaled specimens to permit validation of the scaling parameters and to identify any "scale effects" or nonscaled behavior. This approach has been successfully employed with composite structures in studies of transverse impact of beams,[1] tensile strength,[8] and the static and dynamic responses of eccentrically loaded beam columns.[9,10] A second approach is more mechanistic in nature and will be used in the current work. Here, a scale effect is identified as a departure of the response from a known mechanics model, which occurs systematically with specimen size. In contrast to the similitude approach, the mechanistic approach permits "selective scaling" or the evaluation of the response as a subset of the material and/or geometric parameters is varied. This approach may be preferred when there are many variables involved in characterizing the response, and when it is desired to determine the sensitivity of the response to the change in individual variables. An obvious difficulty with this approach is the need to separate genuine scale effects from any inadequacies in the mechanics model being used.

Presented as Paper 91-0912 at the AIAA/ASME/ASCE/AHS/ASC 32nd Structures, Structural Dynamics, and Materials Conference, Baltimore, MD, April 8–10, 1991; received Jan. 14, 1992; revision received April 24, 1992; accepted for publication May 5, 1992.

*Visiting Assistant Professor, Department of Engineering Science and Mechanics.
†Professor, Department of Engineering Science and Mechanics.
‡Head, Aircraft Structures Branch, Structural Mechanics Division. Fellow AIAA.

The geometric and material variables investigated in this study are flange and web widths, flange-to-web corner radius, thickness, and stacking sequence. Response characteristics to be discussed are initial axial stiffness, buckling loads, load redistribution after buckling, and failure loads and mechanisms. A threefold method of investigation has been adopted: analytical, numerical, and experimental. The purpose of the analytical work is to identify parameters which normalize the initial local buckling loads. Finite element models correct deficiencies in the analytical model and also permit extension of the analyses into the postbuckling regime. Finally, a series of experiments provide the essential validation of the scaling parameters identified.

Analytical Model

An analysis is available for the buckling load of a Z-section stiffener with right-angle flange-to-web corners. This analysis, due to Bulson,[11] is based on a classical model of local buckling. The model was extended by Lee[12] to apply to sections comprised of single-layered orthotropic plates. A further generalization has been achieved in the current work for the application to symmetric laminates, albeit with the limitation that bending-twisting coupling is neglected. One-half of the web (from the flange-to-web corner to the web centerline) and one flange are modeled as plate elements. The symmetry of the web about the web center is used to permit modeling of only half of this member. Governing differential equations for each of the two plate elements may be written as

$$D_{11}\frac{\partial^4 w}{\partial x^4} + 2(D_{12} + 2D_{66})\frac{\partial^4 w}{\partial x^2 \partial y^2} + D_{22}\frac{\partial^4 w}{\partial y^4} + N_x\frac{\partial^2 w}{\partial x^2} = 0$$

where D_{ij} ($i, j = 1, 2, 6$) are the orthotropic plate bending stiffnesses, w is the out-of-plane deflection, x and y are longitudinal and transverse in-plane coordinates, respectively, and N_x is the axial load per unit width. Separate displacement functions $w(x, y)$ are assumed in the web and flange of the form:

$$w(x, y) = f(y)\sin\frac{m\pi x}{L}$$

where L is the plate length and m is the number of half-waves in the buckled shape. Use of these displacement functions transforms the two partial differential equations in terms of $w(x, y)$ into two ordinary differential equations in terms of $f(y)$. A general solution of these ordinary differential equations is of the form:

$$f(y) = A_1\cosh\lambda y + A_2\sinh\lambda y + A_3\cos\omega y + A_4\sin\omega y$$

A total of eight boundary and/or compatibility conditions are needed for a specific solution of these two ordinary differential equations. Equilibrium of the bending moments and rotations is enforced at the web-to-flange joints and provides two compatibility conditions. Zero transverse displacement at the flange-to-web joint provides two boundary conditions. For the web, the two remaining boundary conditions are zero transverse slope and shear force due to the state of symmetry which exists along the web centerline. For the flange, the two remaining boundary conditions are zero shear force and bending moment along the free edge. The mathematical statement of these boundary conditions produces a system of eight equations involving the unknown constants $(A_1 - A_4)_{\text{web}}$ and $(A_1 - A_4)_{\text{flange}}$. The final governing or characteristic equation is obtained by setting the determinant of the coefficients of these unknown constants to zero. The resulting equation can be expressed in the form

$$\left[\frac{F(SS\text{-symmetric})}{(F\text{clamped-symmetric})}\right]_{\text{web}} + \frac{B_w}{B_f}\left[\frac{F(SS\text{-free})}{(F\text{clamped-free})}\right]_{\text{flange}} = 0$$

where each function F is the characteristic equation for a plate element subjected to the indicated pair of boundary conditions on the longitudinal edges; SS refers to a simply supported boundary, symmetric refers to the plate edge being in a plane of symmetry, and B_f and B_w refer to the flange and web widths, respectively. Each characteristic equation represents the expanded determinant of the coefficient matrix formed by application of the indicated boundary conditions.

Two nondimensional load parameters were obtained from the analytical model. The two parameters, α and β, are defined as

$$\alpha = N_x B_w^2/\sqrt{D_{11}D_{22}}$$

and

$$\beta = m\pi B_w\{[(D_{33}/D_{22})^2 - D_{11}/D_{22} + (N_x/D_{22})(L/m\pi)^2]^{1/2} - D_{33}/D_{22}\}^{1/2}$$

where $D_{33} = D_{12} + 2D_{66}$. Presentation of buckling data in terms of these parameters is given in the Results and Discussion section.

Numerical Analysis

The ABAQUS finite element code was used for the numerical analyses which were conducted on an Apollo DN4000 work station. Eight and nine-node shell elements with 5 or 6 degrees of freedom per node were used. The elements are shear deformable, based on a first-order shear-deformation theory. Initial buckling loads were determined using an eigenvalue extraction algorithm. Geometrically nonlinear analyses of models with an initial imperfection were performed throughout the load range using a modified Riks procedure.[13] The imperfection was defined as the sum of the first two buckling modes obtained from the eigenvalue analyses. The amplitude of the imperfection was normalized to 5% of the nominal eight-ply laminate thickness of 1 mm.

Experimental Program

The analytical and numerical studies were used to define the specimen geometries for an experimental investigation of local buckling. The specific geometric and material variables considered and the specimen designations are contained in Table 1. The specimen cross section is shown in Fig. 1. The nominal web and flange widths, defined in Fig. 1, range from $B_w = 19.05$ to 44.45 and $B_f = 12.70$ to 31.75 mm, respectively. The corner radii R are 3.175 and 6.35 mm. The lengths were selected to avoid column buckling. The specimens were cut from long section stock fabricated from Hercules, Inc., AS4/3502 graphite-epoxy unidirectional preimpregnated tape. Three stacking sequences were selected: $[\pm 45/0/90]_s$, $[\pm 45/0/90]_{2s}$, and $[+30/0_2/-30]_s$. The $[\pm 45/0/90]_{2s}$ laminate was chosen to investigate the effect of thickness. This laminate is "scaled" on a sublaminate basis to avoid the matrix cracking associated with repeating individual plies.[8] The purpose of the unorthodox $[+30/0_2/-30]_s$ laminate is to assess the generality of the scaling parameters developed for a high degree

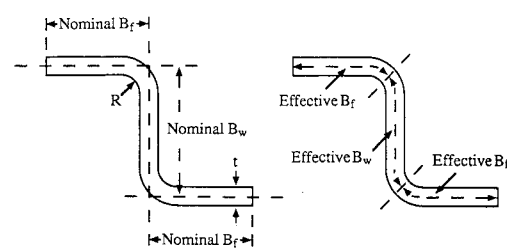

Fig. 1 Definition of nominal and effective geometric parameters.

Table 1 Stiffener geometries and buckling and crippling loads

Specimen type	Number of specimens	Stacking sequence	Web width[a] B_w, mm	Flange width[a] B_f, mm	Corner radius R, mm	Gauge length[b] L, mm	Buckling loads, kN		Crippling loads, kN
							Experiment	FEM[c]	Experiment
Z1	3	$[\pm 45/0/90]_{2s}$	44.45	31.75	3.175	254	35.1	36.2	49.9
Z2	3			25.40			45.0	43.5	52.3
Z3	3			19.05		152	57.2	57.1	59.0
Z4	2	$[\pm 45/0/90]_s$	44.45	31.75	3.175	254	4.5	4.7	16.1
Z5	2			25.40			5.7	6.0	16.2
Z6	2			19.05		152	7.9	8.1	14.4
Z7	2			12.70			7.9	8.2	13.4
Z8	3	$[30/02/-30]_s$	44.45	31.75	3.175	254	3.1	3.2	12.3
Z9	3			25.40			3.9	4.0	12.3
Z10	3			19.05		152	5.5	5.5	13.5
Z11	3			12.70			5.7	5.4	12.7
Z12	2	$[\pm 45/0/90]_s$	31.75	31.75	3.175	254	4.1	4.2	17.3
Z13	3			25.40			5.3	5.5	16.5
Z14	3			19.05		152	7.8	7.9	15.2
Z15	2			12.70			11.1	11.1	13.7
Z16	3	$[\pm 45/0/90]_s$	31.75	31.75	6.35	254	4.8	4.7	18.7
Z17	2			25.40			6.3	6.3	17.1
Z18	2			19.05		152	9.4	9.5	15.4
Z19	2			12.70			12.8	13.4	14.5
Z20	2	$[\pm 45/0/90]_s$	19.05	19.05	3.175	152	6.9	7.2	11.0
Z21	2			12.70			10.3	10.4	11.0

[a]Nominal dimensions. See Fig. 1 for definitions.
[b]Each specimen had an additional 25.4 mm of length supported by potting material at each end.
[c]FEM = finite element method.

of orthotropy and bending-twisting coupling. The bending-twisting coupling was not included in the analytical formulation. The ends of the specimens were potted in an aluminum-filled epoxy compound to a depth of 25.4 mm, and contained by steel or aluminum rings of 100–125 mm diameter. These potted end supports provide for uniform load introduction, prevent end brooming of the specimens under compression, and simulate clamped boundary conditions.

Back-to-back strain-gauge pairs were located at axial positions corresponding to the numerically predicted locations of the antinodes of the first two buckling modes. Longitudinal strain-gauge pairs were located at the flange-free edge, mid-flange, flange-to-web corner, and midweb locations. Transverse strain-gauge pairs were located at the flange-to-web corner and midweb locations. The strain gauges aided in the determination of initial buckling and revealed the nature of the load redistribution after buckling. Direct Current Displacement Transducers (DCDTs) were placed near the flange-free edges at three or four locations per flange to measure out-of-plane displacements. Specimen end shortening was also measured with DCDTs. In addition, one flange was monitored using a shadow moire technique to aid in the determination of the onset of buckling and the resulting mode shape. Specimens were loaded at a nominal axial strain rate of 0.001 min^{-1} between aligned platens of a 534-kN-capacity hydraulic testing machine at NASA Langley Research Center.

Results And Discussion

Prebuckling

Prior to buckling, a state of approximately uniform compression is assumed to exist in the specimens. A plot of the load normalized by the cross-sectional area and the equivalent longitudinal modulus vs the end shortening normalized by the length (P/AE vs U/L) should have a unit slope prior to buckling. However, the experimentally observed slopes range from 0.87 to 1.02. Potential sources of error are the values of P, A, E, U, and L which were used. The accuracy of the load P and end shortening U measurements is considered satisfactory. The cross-sectional area A was calculated based on the actual stiffener dimensions. The equivalent longitudinal moduli in compression E were measured using coupons cut from the Z-section stock, and were found to be 4 to 6% lower than predicted from lamination theory using nominal ply properties of $E_1 = 127.5$ GPa, $E_2 = 11.31$ GPa, $G_{12} = 6.0$ GPa, and $\nu_{12} = 0.3$.[3] Therefore, the value of the equivalent longitudinal moduli may account for up to one-half of the observed discrepancy. An additional source of error in prebuckling stiffness is the effective length of the stiffener. The effective length is in between the total length and the gauge length due to the fact that some displacement can occur within the potted end supports. The total depth of the end supports is either 20% or 33% of the gauge length, as indicated in Table 1.

The constraint offered by the potted end supports varied as a function of specimen geometry and stacking sequence. A qualitative prediction of the behavior can be obtained from the following model. The total end shortening between the platens of the test machine can be expressed as $U = U_g + U_p$, where U_g and U_p are the net shortening of the specimen which occurs in the gauge length and potted end supports, respectively. The displacement in the gauge length satisfies the equation $P/AE = U_g/L$, where P, A, and E are the load, cross-sectional area, and equivalent longitudinal modulus from lamination theory, respectively. The shortening in the potted end supports may be represented as $U_p = kL_pP/s$, where k is a potted end support parameter (composed of an inverse modulus and a characteristic length), L_p is the sum of the depths of the potted end supports, and s is the total width of the developed cross section of the stiffener. Combining the above yields

$$P/AE = (U - U_p)/L = U/[L + kEtL_p] = n(U/L)$$

where

$$n = 1/[1 + (kEtL_p)/L]$$

and the cross-sectional area A is equal to $(s\,t)$, for laminate thickness t. The model predicts that the effect of the potted end supports on axial stiffness of the complete potted specimen should increase with increasing laminate thickness and decreasing gauge length, and be independent of flange or web widths. The model suggests that a plot of $1/n = (U/L)/(P/AE)$ vs (EtL_p/L) would produce a line of slope k and an intercept of 1. Such a plot is contained in Fig. 2 using the experimentally observed "n" values. The dependence of the data on the parameters E, t, and L is generally consistent with the trends predicted by the model. However, the model does not predict the exact functional dependence of the behavior,

nor the large differences among replicate specimens. Some variation in the response between replicate specimens of the $[+30/0_2/-30]_s$ stacking sequence is attributed to an initial lack of parallelness between the two surfaces of the potted end supports in contact with the platens of the test machine, as indicated by strain-gauge data. The compression and shear stress-strain behavior of the potting compound were measured using specimens cut from a potted end support near the interface with the stiffener. Significant nonlinearity in both the compression and shear responses indicates that the parameter k in the above model is not a material constant. Indeed, the differing stress levels in the end supports among the various specimens gives further cause for the observed varying effect of the end supports on axial stiffness.

The displacement occurring in the end supports will influence the apparent axial stiffness of a specimen throughout the entire load range, and not just prior to buckling. The significance of the above discussion is that an experimental artifact such as these potted end supports might result in an apparent size dependence of the overall structural response. This might be interpreted falsely as a scale effect if the mechanics governing the constraint of the potted end supports are not included in the analyses.

Initial Local Buckling

Measured and predicted initial buckling loads for the Z-section stiffeners presented in this study are contained in Table 1. Nondimensionalization of the governing equations revealed two normalizing parameters α and β defined previously in the Analytical Model section. The first parameter α normalizes the buckling load per unit cross-sectional width N_x in terms of the web width and the axial and transverse bending stiffnesses. The buckling loads of the specimens in this study normalized in this fashion are shown in Fig. 3, plotted against the nominal flange-to-web width ratio B_f/B_w. The results for three web widths and two quasi-isotropic stacking sequences are contained in the figure. The parameter α normalizes the buckling data for the various web widths, but not for the different stacking sequences. The agreement between the experimental values and the corresponding finite element predictions shown in the figure is good. The data indicate that sections with a B_f/B_w ratio greater than 0.2–0.25 are flange critical; that is the flange is too wide to provide efficient stiffening of the web without the flange buckling. The effect of the larger corner radius is to increase the buckling loads by 13 to 17%. The agreement between the analytical model and the experiments improves as the true cross-sectional geometry approaches the idealized model; that is as the corner radius decreases. The agreement between the experiments and the analytical model degrades as the B_f/B_w ratio is decreased. This result is to be expected since the analytical model assumes a right-angle corner, and the actual curved corner of the specimen becomes a relatively greater portion of the cross section as the flange width is reduced. This is, therefore, not a scale effect per se, but rather an example of a deficiency in the model being used to evaluate the behavior.

The second parameter β normalizes the buckling load per unit cross-sectional width N_x in terms of the web width, specimen gauge length, the number of half-waves in the buckled mode shape, and all of the bending stiffnesses except D_{16} and D_{26}. The parameter β effectively normalizes the buckling data for all of the geometric and material variables included in the model, as shown in Fig. 4a in which β is plotted against the flange-to-web width ratio B_f/B_w for the specimens in the current study. The normalization is based on the effective flange and web widths, which are defined as the sum of the flat portions of the respective elements with one-half of the centerline arclength of the adjacent corner (see Fig. 1). The parameter β is also plotted against B_f/B_w in Fig. 4b for data in the literature.[2-6] A corner radius of 3.175 mm was assumed when one was not stated in the references. The data in Fig. 4b cover a range of materials and laminate stacking sequences and are for the most part from channel section stiffeners, rather than Z-section stiffeners. The analytical model, however, applies equally to both cross sections. The agreement is good, particularly in view of the variability in specimen preparation, end supports, and test procedures which likely exists. As discussed above, the analytical and experimental agreement degrades as the flange width is reduced. The use of the effective flange and web widths unifies the data for the two corner radii considered in the current study. In summary, the parameter β is an effective parameter for the scaling of the initial local buckling loads of laminated composite Z-section stiffeners.

A Ritz analytical model for predicting buckling loads is also presented in Ref. 4. The model treats the stiffener as being comprised of individual plate elements which are simply supported at the plate junctions. This choice of boundary condition at the junctions enables the bending-twisting coupling to be more readily included in the model. Therefore, the models of Ref. 4 and the present paper represent two different compromises (flange-to-web boundary conditions vs bending-twisting coupling) for buckling load prediction. The implications of the different assumptions will now be discussed. Estimated buckling loads in Ref. 4 for channel sections were below experimental values by 19% and 7.5% on average for the assumptions of simply supported and clamped boundary conditions on the loaded edges, respectively. The underestimation of the buckling loads was attributed to the assumption of simply supported conditions at the flange-to-web junctions.[4] Finite element analyses of the sections in the current study were performed with and without the Q_{16} and Q_{26} stiffness

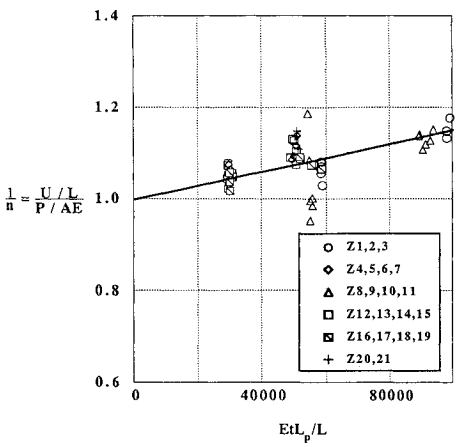

Fig. 2 Correlation of model for initial axial stiffness with experimental data.

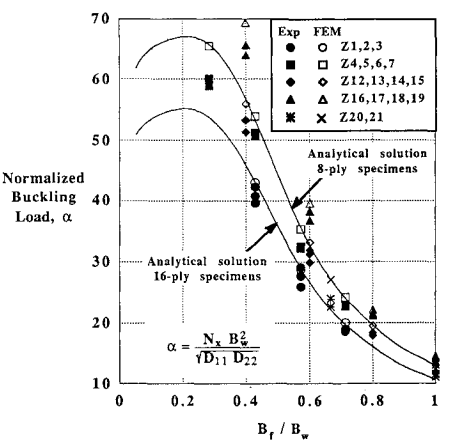

Fig. 3 Normalized buckling loads in terms of parameter α.

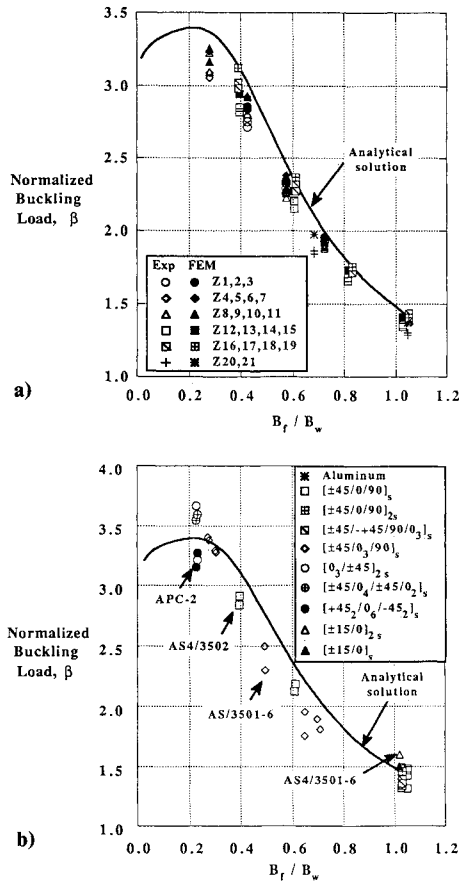

Fig. 4 Normalized buckling loads in terms of parameter β: a) data from current work, and b) data from Refs. 2–6.

coupling terms included to evaluate the implications of neglecting the bending-twisting coupling in the analytical model. For the case of a 44.45-mm-wide web and 31.75-mm-wide flange, the calculated buckling loads are 0.6%, 4.0%, and 16% higher when $Q_{16} = Q_{26} = 0$ for laminates $[\pm 45/0/90]_{2s}$, $[\pm 45/0/90]_s$, and $[+30/0_2/-30]_s$, respectively. The ratio of bending stiffnesses D_{16}/D_{11} for these cases are 0.06, 0.16, and 0.21, respectively. These results indicate that the impact of neglecting the coupling terms on the buckling loads increases in proportion to the relative magnitude of this coupling.

Postbuckling

The partitioning of the total load carrying range between the prebuckling and postbuckling regimes depends on the section geometry and stacking sequence. Pertinent parameters discussed in previous work on stiffener crippling are the flange-to-web width ratio B_f/B_w and width-to-thickness ratios B_f/t and B_w/t. A more general parameter for ranking the load-end shortening responses of the various section geometries is a normalized width, defined as the ratio of the total width of the cross section s, which is approximately $(2B_f + B_w)$ and the section thickness t (see Fig. 1). The load-end shortening responses of selected specimens are illustrated in Fig. 5. These specimens represent a range of flange, web, and thickness dimensions. The applied load P is normalized by the extensional modulus E and cross-sectional area A. The end shortening U is normalized by the stiffener gauge length L. The normalized widths s/t for these specimens are identified in the figure. The results indicate that specimens having a large s/t ratio are relatively wide and thin, and, therefore, buckle at lower stresses, but have an extensive postbuckling load range. For smaller normalized widths, buckling occurs at higher stresses, and the postbuckling range is reduced. The increased buckling resistance for decreasing flange width is expected, since all of the specimens in this study are predicted to be flange critical to varying degrees. The effect of decreasing the web width is also to increase the buckling and postbuckling stresses. This increase results from the web becoming relatively thicker (due to decreasing width-to-thickness ratio B_w/t) as the web is reduced. The effect of thickness is most noticeable since the bending stiffnesses increase proportionally with t^3. The result is that buckling loads increase by a factor of approximately eight with a doubling of the laminate thickness. Postbuckling loads remain significantly higher, as well. The figure also indicates that the range of postbuckling response is significantly reduced for the thicker specimens.

After buckling, the axial compressive load is no longer distributed uniformly over the cross section. The redistribution of load results from the reduced axial stiffness associated with bending in the flanges and web. The corner regions remain nominally straight and unbuckled, and, therefore, load tends to concentrate there. The redistribution of load will influence local stress states which may be related to final failure. The rate at which the redistribution occurs with continued loading in the postbuckling regime will, therefore, affect the total extent of the postbuckling load range and the mode of failure. The nature of this load redistribution can be evaluated using the data from strain gauges located over the cross section. The redistribution of strain across the cross section is shown in Fig. 6 for sections of various web, flange, and thickness dimensions. The data presented in Fig. 6 are for applied postbuckling loads corresponding to average strains (U/L) 0.3% above the strains at buckling. These loads were selected so that the rate of strain redistribution could be evaluated as a function of the geometric parameters. The ordinate in Fig. 6 is the membrane strain (the average of front and back

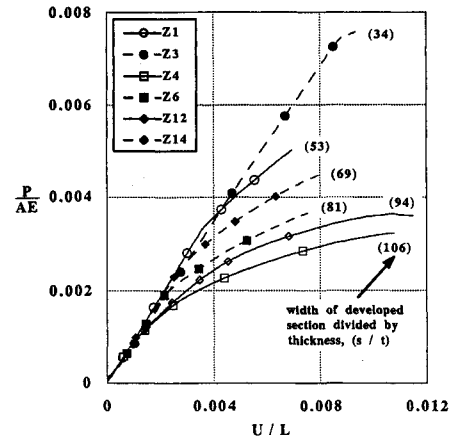

Fig. 5 Experimental load-end shortening results.

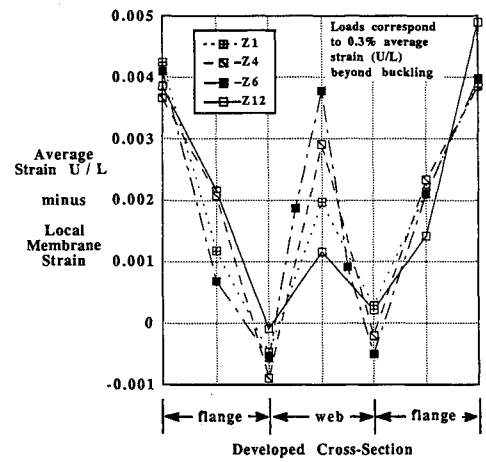

Fig. 6 Strain redistribution due to buckling.

strain-gage pairs), at some position in the developed cross section, shifted by the average strain U/L as a reference value. Thus, the plotted strains represent departures, due to buckling, from uniform uniaxial membrane behavior. Specifically, a strain of zero in the figure means that the actual strain at that location is the same as the average value. The strain-gauge data are from axial locations corresponding to antinodes of the buckled stiffener. Specimens Z4 and Z6 are compared first to examine the effect of flange width. Buckling of the flanges results in their being unloaded at the edges to approximately the same degree. Specimen Z6 should have larger displacements in the web since it is relatively less flange critical due to its narrower flanges. This response is manifested by an unloading at the web center that is almost equal to that of the flange-free edges. In contrast, the center of the web of specimen Z4 (with wider flanges) is unloaded to a lesser degree as a result of buckling. The significant unloading of both specimens at the flange-free edges results in the transfer of load to the corner regions. Membrane strains in the corners are slightly greater than the average values. The effect of web width (31.75 mm vs 44.45 mm) is illustrated by specimens Z12 and Z4, respectively. The 31.75-mm-wide flanges of both specimens again unload to approximately the same degree. Here, however, the narrower web has greater bending stiffness due to its smaller B_w/t ratio. It retains, therefore, much more membrane stiffness than the wider web. The consequence of the higher membrane stiffness is that less strain concentration occurs in the corners, compared to specimen Z4. Finally, the effect of thickness is shown by comparing the results for specimens Z4 and Z1. The web and flange widths are 44.45 mm and 31.75 mm, respectively, for both specimens. Once again, the flanges are unloaded to the same degree. In this case, the lower B_f/t and B_w/t occur in specimen Z1 due to the greater laminate thickness. The thicker specimen retains more membrane stiffness in the web and undergoes less strain concentration in the corners, although both effects occur to a lesser degree than for the case of a reduced B_w/t due to a narrower web, as shown by the results for specimen Z12. Note that the B_w/t ratios for specimens Z4, Z1, and Z12 are 44, 22, and 31, respectively. In comparing the effects of web width and thickness on strain redistribution, it is apparent that the former is more significant.

Crippling

The complex interaction between the overall structural deflections and the localized, material-induced deformation makes crippling the most difficult of the response mechanisms to characterize. Nominal crippling stresses can be related to the normalized total width s/t. The nominal buckling and crippling stresses P/A of all specimens are plotted against s/t in Fig. 7. Buckling occurs at low stresses for high values of normalized total width s/t. The resulting redistribution of strain and the reduction in stiffness caused by buckling limit the ultimate or crippling stress to low values. As the normalized total width decreases, the buckling stresses increase. Once buckling occurs, however, the reduction in stiffness and the redistribution of strain are more severe as discussed in the previous section on postbuckling. Therefore, the increment in stress between buckling and crippling is reduced, albeit the absolute crippling stress is increased. In the absence of a competing mode, the local buckling and failure stresses converge as s/t is decreased. The figure also contains data from Ref. 2 for the short-column material failure of a $[\pm 45/0/90]_{2s}$ AS4/3502 Z-section stiffener with a 31.75-mm-wide web and a 19.05-mm-wide flange. The normalized width of this specimen in the figure is reduced to the point where a material limit in compression is reached before or simultaneously with buckling.

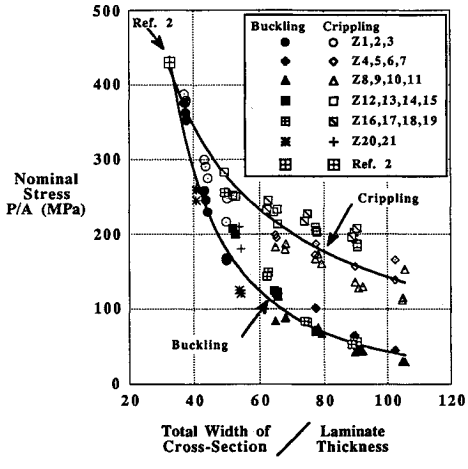

Fig. 7 Buckling and crippling stress summary.

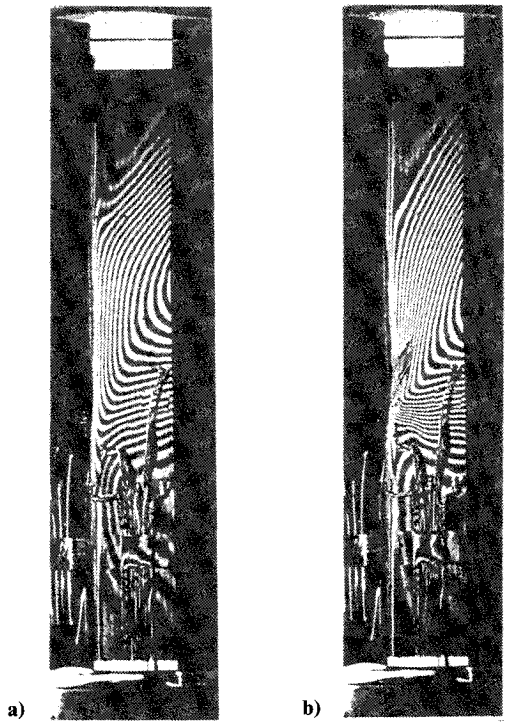

Fig. 8 Shadow moire fringe patterns of flange for $[+30/0_2/-30]_s$ specimen type Z8 at axial load: a) 11.1 kN; and b) 12.2 kN.

The precise failure mechanisms responsible for crippling could not be isolated in general, due to the presence of secondary laminate damage caused by the load redistribution following the primary failure event. Two failure mechanisms discussed in previous work on composite stiffener crippling (e.g., Refs. 3, 4, and 7) are flange-free edge delamination and crushing or material failure in the flange-to-web corner. A third crippling mode is a transverse shear or skin rupturing mode, which has been observed to occur at nodal positions in buckled plates.[14] The crippling responses of the specimens in the current work depend on the stacking sequence, and range from flange-free edge delamination with essentially no fiber fractures to localized failure in the corner regions with no free-edge delamination. Failure in the $[+30/0_2/-30]_s$ specimens occurred near the flange-to-web corners at antinodes of the buckled mode shape. The shadow moire fringe patterns on the flanges of these specimens were distorted into a series of chevron-like shapes, as shown in Fig. 8a. The midpoints of these chevrons form the locus of points defining the location of the antinode over the width of the flange. The pointedness of the fringes indicated the presence of large bending curvature along the antinode. Surface ply cracking transverse to the

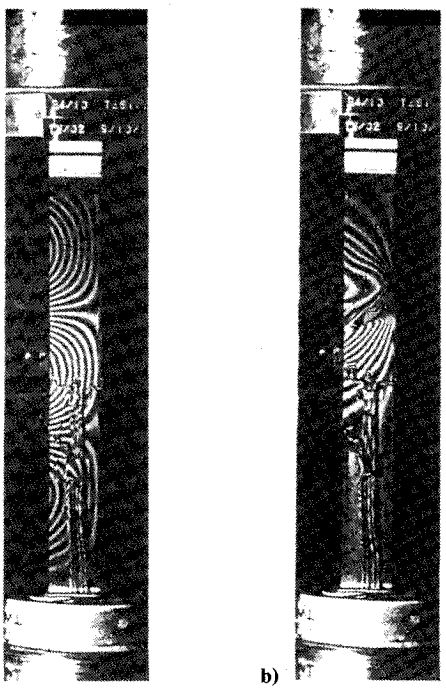

Fig. 9 Shadow moire fringe patterns of flange for $[\pm 45/0/90]_{2s}$ specimen type Z1 at axial load: a) 49.0 kN, and b) 53.2 kN.

fiber direction occurred along the antinode near the flange-to-web corner, as shown in Fig. 8b. The distortion of the fringe pattern is indicative of twisting of the section. Numerical postbuckling analyses performed with and without the bending-twisting coupling that is present in this laminate indicate that the distortion of the mode shape is due to this coupling. The numerical analyses further predict tensile matrix stresses in the surface plies exceeding twice a nominal strength of 51.7 MPa.[15] Strain gauges also detected the presence of large transverse tensile strains in the corners. These strains are a consequence of the low bending stiffness for this stacking sequence in the transverse direction. Flange-free edge delamination was only observed in the $[+30/0_2/-30]_s$ specimens with the smallest flanges. These observations indicate that failure in these specimens was precipitated by local failure in the corners due to in-plane shear and/or matrix cracking.

Failure of specimens fabricated from the 16-ply quasi-isotropic laminate was dominated by flange-free edge delamination. Some specimens exhibited only this delamination, with no fiber fractures. The shadow moire fringe patterns did not indicate the presence of twisting (Fig. 9a). Less twisting would be expected in this case since the D_{16} and D_{26} are only 6% of D_{11}, in contrast to the $[+30/0_2/-30]_s$ specimens where D_{16} is 21% of D_{11}. Failures occurred in both nodal and antinodal axial locations. A nodal crippling mode is illustrated in Fig. 9b. The numerical postbuckling analyses for the $[\pm 45/0/90]_{2s}$ specimens predict a less severe in-plane stress state at crippling, with stresses rarely exceeding nominal strength values. The nature of the crippling damage and the stress analyses indicates that failure of the $[\pm 45/0/90]_{2s}$ specimens was dominated by the out-of-plane stress state.

The failure of the eight-ply quasi-isotropic specimens included the features of both flange-free edge delamination and local failure in the corners. Delamination was more prevalent in the specimens having smaller flanges. Corner crushing was more prevalent in specimens with larger flanges. An intermediate amount of twisting was observed, compared to the other two laminates. The D_{16} and D_{26} are 16% of D_{11} for the eight-ply quasi-isotropic laminate. Significant variability in the extent of the postbuckling responses among replicate specimens was also observed. The range of end shortening values at crippling was 50% of the average value among geometries Z4 and Z5.

Concluding Remarks

The buckling, postbuckling, and crippling of Hercules, Inc., AS4/3502 graphite-epoxy Z-section stiffeners have been discussed in the context of scaling considerations. The approach to scaling used in this investigation has been to evaluate the behavior relative to known mechanics models, as one or more of the geometric and material variables were varied. This approach is in contrast to the more traditional approach of using dimensional analysis to produce a series of experiments in which all parameters are scaled simultaneously. Two nondimensional parameters have been identified from an analytical model which normalize the buckling data. One parameter normalizes buckling data for various web widths only. The other parameter normalizes data for various web, flange, and thickness dimensions, and stacking sequences and material systems. The agreement between the analytical and experimental buckling loads is generally good. The agreement degrades as the flange-to-web width ratio is reduced and as the section corner radius is increased, since the actual finite radius corners represent a departure from the right-angle corners assumed in the analytical model. The actual corners constitute an increasing portion of the cross section as the flange-to-web width ratio is reduced and as the corner radius is increased. The variation in the agreement between the analytical and experimental results with the flange-to-web width ratio and the corner radius is therefore not a scale effect per se, but the result of a deficiency in the model being used to judge the behavior. Buckling results in load redistribution across the cross section. The flange-free edges and web centers typically unload, with strain being concentrated in the nominally straight, unbuckled corner regions. The severity of this redistribution increases as the flange-to-web width ratio decreases and as the web width-to-thickness ratio increases. Crippling stresses are correlated with the ratio of the total cross section centerline width to the section thickness. Buckling stresses decrease, but the increment in stress between buckling and crippling increases as the total width normalized by the thickness increases. Buckling and crippling stresses converge as the normalized total width decreases. The crippling mechanisms depend on the stacking sequence and include flange-free edge delamination and local failure in the flange-to-web corner.

Acknowledgment

A part of this work was sponsored by the NASA Langley Research Center under Grant NAG-1-343 (NASA-Virginia Tech Composites Program).

References

[1]Morton, J., "Scaling of Impact Loaded Fiber Composites," *AIAA Journal*, Vol. 26, No. 8, 1988, pp. 989–994.

[2]Tyahla, S. T., and Johnson, E. R., "Failure and Crippling of Graphite-Epoxy Stiffeners Loaded in Compression," Virginia Polytechnic Inst. and State Univ., Blacksburg, VA, CCMS-84-07 and VPI-E-84-19, June 1984.

[3]Bonanni, D. L., Johnson, E. R., and Starnes, J. H., Jr., "Local Crippling of Thin-Walled Graphite-Epoxy Stiffeners," *AIAA Journal*, Vol. 29, No. 11, 1991, pp. 1951–1959.

[4]Causbie, S. M., and Lagace, P. A., "Buckling and Final Failure of Graphite/PEEK Stiffener Sections," AIAA Paper 86-0921; *Proceedings of AIAA/ASME/ASCE/AHS 27th Structures, Structural Dynamics, and Materials Conference* (San Antonio, TX), May 1986, pp. 280–287.

[5]Wang, C., Pian, T. H. H., Dugundji, J., and Lagace, P. A., "Analytical and Experimental Studies on the Buckling of Laminated Thin-Walled Structures," AIAA Paper 87-0727; *Proceedings of AIAA/ASME/ASCE/AHS 28th Structures, Structural Dynamics, and Materials Conference* (Monterey, CA), April 1987, pp. 135–140.

[6]Spier, E. E., "Postbuckling Fatigue Behavior of Graphite-Epoxy Stiffeners," AIAA Paper 82-0779; *Proceedings of AIAA/ASME/ASCE/AHS 23th Structures, Structural Dynamics, and Materials*

Conference (New Orleans, LA), May 1982, pp. 511–527.

[7]Rehfield, L. W., and Reddy, A. D., "Observations on Compressive Local Buckling, Postbuckling and Crippling of Graphite/Epoxy Airframe Structure," AIAA Paper 86-0923; *Proceedings of the AIAA/ASME/ASCE/AHS 27th Structures, Structural Dynamics, and Materials Conference,* (San Antonio, TX) May 1986, pp. 301–306.

[8]Kellas, S., and Morton, J., "Strength Scaling in Fiber Composites," *AIAA Journal,* Vol. 30, No. 4, 1992, pp. 1074–1080.

[9]Jackson, K. E., and Fasanella, E. L., "Scaling Effects in the Static Large Deflection Response of Graphite-Epoxy Composite Beams," NASA TM 101619, June 1989.

[10]Jackson, K. E., and Fasanella, E. L., "Scaling Effects in the Impact Response of Graphite-Epoxy Composite Beams," *Society of Automotive Engineers Technical Paper Series,* Paper 891014, April 1989, pp. 1–14.

[11]Allen, H. G., and Bulson, P.S., *Background to Buckling,* McGraw-Hill Book Co., (UK) Ltd., Maidenhead-Berkshire, 1980, Chap. 5.

[12]Lee, D. J., "The Local Buckling Coefficient for Orthotropic Structural Sections," *Aeronautical Journal,* Vol. 82, No. 811, July 1978, pp. 313–320.

[13]Crisfield, M. A., "A Fast Incremental/Iteration Solution Procedure that Handles Snap-Through," *Computers and Structures,* Vol. 13, June 1981, pp. 55–62.

[14]Starnes, J. H., Jr., and Rouse, M., "Postbuckling and Failure Characteristics of Selected Flat Rectangular Graphite-Epoxy Plates Loaded in Compression," AIAA Paper 81-0543; *Proceedings of AIAA/ASME/ASCE/AHS 22th Structures, Structural Dynamics, and Materials Conference* (Atlanta, GA), April 1981, pp. 423–434.

[15]Tsai, S. W., *Composites Design,* 4th ed., Think Composites, Dayton, Ohio, 1988, p. 11-8.